THE GEOLOGICAL SOCIETY OF AMERICA®

Isotopic signature of dissolved iron delivered to the Southern Ocean from hydrothermal vents in the East Scotia Sea

Jessica K. Klar[1]*, Rachael H. James[1], Dakota Gibbs[2,3], Alastair Lough[1], Ian Parkinson[4], J. Andrew Milton[1], Jeffrey A. Hawkes[5], and Douglas P. Connelly[2]

[1]Ocean and Earth Science, University of Southampton Waterfront Campus, National Oceanography Centre Southampton, European Way, Southampton SO14 3ZH, UK

[2]Marine Geosciences, National Oceanography Centre Southampton, European Way, Southampton SO14 3ZH, UK

[3]Southern Cross Geoscience, Military Road, Lismore, NSW 2480, Australia

[4]School of Earth Sciences, University of Bristol, Queens Road, Bristol, BS8 1RJ, UK

[5]Department of Chemistry, Uppsala University, SE-751 05 Uppsala, Sweden

ABSTRACT

It has recently been demonstrated that hydrothermal vents are an important source of dissolved Fe (dFe) to the Southern Ocean. The isotopic composition (δ^{56}Fe) of dFe in vent fluids appears to be distinct from other sources of dFe to the deep ocean, but the evolution of δ^{56}Fe during mixing between vent fluids and seawater is poorly constrained. Here we present the evolution of δ^{56}Fe for dFe in hydrothermal fluids and dispersing plumes from two sites in the East Scotia Sea. We show that δ^{56}Fe values in the buoyant plume are distinctly lower (as low as −1.19‰) than the hydrothermal fluids (−0.29‰), attributed to (1) precipitation of Fe sulfides in the early stages of mixing, and (2) partial oxidation of Fe(II) to Fe(III), >55% of which subsequently precipitates as Fe oxyhydroxides. By contrast, the δ^{56}Fe signature of stabilized dFe in the neutrally buoyant plume is −0.3‰ to −0.5‰. This cannot be explained by continued dilution of the buoyant plume with background seawater; rather, we suggest that isotope fractionation of dFe occurs during plume dilution due to Fe ligand complexation and exchange with labile particulate Fe. The δ^{56}Fe signature of stabilized hydrothermal dFe in the East Scotia Sea is distinct from background seawater and may be used to quantify the hydrothermal dFe input to the ocean interior.

INTRODUCTION

The Southern Ocean is of significant importance to the global carbon cycle and is a major sink for atmospheric carbon dioxide (CO_2) (Pollard et al., 2009). The micronutrient iron (Fe) is a key regulator of primary productivity and therefore CO_2 uptake in the Southern Ocean (e.g., Martin et al., 1990). The impact of past and future climate variability has been shown to be mediated by modifications to the supply of Fe to the biota in this area (e.g., Watson et al., 2000). Understanding the pathways that govern Fe supply to and removal from the Southern Ocean is therefore critical to quantifying the impact of Fe on global productivity. However, the relative importance of different sources of Fe to the oceans is not well known, and flux estimates from atmospheric dust, hydrothermal vents, icebergs, and oceanic sediments vary by orders of magnitude (Boyd and Ellwood, 2010).

A number of recent studies have demonstrated that as much as 46% of hydrothermal Fe may remain in the dissolved (<0.2 µm) phase, in the form of either colloids or organic complexes (Bennett et al., 2008; Hawkes et al., 2013, 2014; Saito et al., 2013; Fitzsimmons et al., 2014; Kleint et al., 2016). In support of this, modeling studies have shown that observations of the distribution of dissolved Fe (dFe) in the Southern Ocean can only be replicated when the Fe flux from hydrothermal sources is included (Tagliabue et al., 2010, 2014), and analyses of dFe on transects across the North Atlantic, South Atlantic, and eastern equatorial Pacific have provided evidence for advection of hydrothermal dFe for thousands of kilometers away from the mid-ocean ridge (Saito et al., 2013; Conway and John, 2014; Fitzsimmons et al., 2014; Resing et al., 2015).

Attempts have been made to parameterize hydrothermal dFe using dissolved Fe/^{3}He ratios, but this approach is imprecise because hydrothermal fluids have widely variable Fe/^{3}He (Tagliabue et al., 2010; Saito et al., 2013). Moreover, the controls on the proportion of hydrothermal Fe that is stabilized in the dissolved phase are unknown (Kleint et al., 2016). In principle, one way to circumvent some of these problems is by analysis of stable Fe isotopes. However, δ^{56}Fe values of dFe {δ^{56}Fe, where $\delta^{56}Fe = [(^{56}Fe/^{54}Fe)_{sample} / (^{56}Fe/^{54}Fe)_{IRMM\text{-}14} - 1] \times 1000$; IRMM—Institute for Reference Materials and Measurements} proximal to vent sites vary from −1.35‰ to +0.56‰ (Conway and John, 2014; Fitzsimmons et al., 2016), whereas δ^{56}Fe values reported for hydrothermal fluids range from −0.69‰ to +0.28‰ (Beard et al., 2003; Severmann et al., 2004; Rouxel et al., 2008, 2016; Bennett et al., 2009). The likely reason for this is that the δ^{56}Fe composition of hydrothermal dFe is modified on mixing with seawater due to precipitation of Fe sulfides, oxidation of Fe(II) to Fe(III), and Fe(III)-oxyhydroxide formation (e.g., Welch et al., 2003; Rouxel et al., 2008, 2016; Bennett et al., 2009; Roy et al., 2012).

Here we study the evolution of δ^{56}Fe during mixing between hydrothermal fluids and seawater, presenting the first compilation of δ^{56}Fe in hydrothermal fluids, buoyant and nonbuoyant plumes at two vent sites, E2 and E9N, located on the East Scotia Ridge (see the GSA Data Repository[1] for sample site descriptions and sampling strategies). We use these data to determine the controls on the isotopic signature of hydrothermal dFe delivered to the Scotia Sea in the Southern Ocean and show that Fe isotopes are likely to be effective tracers of hydrothermal dFe throughout most parts of the world oceans.

RESULTS

Vent fluids with minimal seawater mixing (Mg < 1.64 mM) display Fe concentrations of 1070 µM at Site E2 and 580 µM at E9N, and have similar δ^{56}Fe values (−0.28‰ at E2 and −0.30‰ at E9N). Water samples obtained from the buoyant part of the hydrothermal plume have the lowest δ^{56}Fe values (as low as −1.19‰ at E2 and as low as −0.76‰ at E9N)

*Current address: LEGOS, University of Toulouse, IRD, CNES, CNRS, UPS, 18 avenue Edouard Belin, 31401 Toulouse, France; E-mail: Jessica.klar@legos.obs-mip.fr.

[1]GSA Data Repository item 2017101, supplemental information on study area, methods, isotope modeling, and data, is available online at http://www.geosociety.org/pubs/ft2017.htm or on request from editing@geosociety.org.

and highest dFe concentrations (as high as 83.5 nM at E2 and as high as 23.0 nM at E9N; Fig. 1). As the hydrothermal plume is dispersed and further diluted in the neutrally buoyant part of the hydrothermal plume, dFe concentrations decrease, whereas δ^{56}Fe values increase. Slight differences in δ^{56}Fe values and dFe concentrations can be observed between the two vent sites: for the same degree of dilution, samples from E9N tend to have slightly higher δ^{56}Fe and lower dFe compared to samples from E2. Total (dissolved + particulate) concentrations of Fe (tFe) are, on average, 40% ± 10% and 70% ± 30% lower at E2 and E9N, respectively, than calculated, assuming that Fe is conserved during mixing between the end-member vent fluid and seawater (Fig. 1). Partitioning of Fe between different size fractions, and δ^{56}Fe values, may, however, be slightly modified in the interval between sampling and processing (see the Data Repository).

DISCUSSION

The missing tFe is likely to have been removed by precipitation of iron sulfides immediately on venting at the seafloor (e.g., Rudnicki and Elderfield, 1993), and higher Fe sulfide removal at E9N may be due to the slightly higher sulfide concentrations found in E9N vent fluids (James et al., 2014). Field and experimental studies have shown that light Fe isotopes are preferentially incorporated into Fe sulfides, leaving the remaining dFe isotopically heavy (Rouxel et al., 2008, 2016; Bennett et al., 2009; Roy et al., 2012). Assuming that the fractionation factor associated with Fe sulfide formation [$\Delta_{Fe(II)\text{-}FeS}$] is +0.66‰ (Rouxel et al., 2008; Bennett et al., 2009; Roy et al., 2012), then according to the Rayleigh fractionation model, the δ^{56}Fe value of the remaining dFe would be +0.07‰ ± 0.05‰ at E2 and +0.49‰ ± 0.05‰ at E9N. Assuming that a small part (<10%) of the dFe in the buoyant plume may be present as pyrite nanoparticles (Yücel et al., 2011) that would contribute light isotopes to the dissolved fraction, this would still produce δ^{56}Fe values (–0.02‰ at E2, +0.39‰ at E9N) that are higher than we measure in the buoyant plumes.

The low Fe isotopic values in the buoyant part of the plume are, however, consistent with Fe sulfide formation combined with partial oxidation of Fe(II) to Fe(III). Oxidation of Fe(II) to Fe(III) results in enrichment of the heavy Fe isotopes in Fe(III) such that the δ^{56}Fe value of the remaining Fe(II) is up to 3.56‰ lower than Fe(III) (Welch et al., 2003). Fe(III) is not stable in seawater and rapidly forms Fe(III) oxyhydroxides, which tend to aggregate and coagulate into larger particles (Field and Sherrell, 2000; Statham et al., 2005). Because these heavy Fe(III) oxyhydroxide particles are no longer part of the dFe fraction (<0.2 µm), the δ^{56}Fe value of the remaining dFe pool decreases (e.g., Severmann et al., 2004; Bennett et al., 2009; Rouxel et al., 2016).

The evolution of δ^{56}Fe in the buoyant plumes at E2 and E9N after sulfide formation is complete can therefore be modeled as a function of the proportion of Fe(II) oxidized to Fe(III) and the proportion of Fe(III) that leaves the dissolved phase (i.e., coagulates to form particles larger than 0.2 µm) (Fig. 2; see the Data Repository for a detailed description). According to the model, the δ^{56}Fe values measured in the buoyant plume are consistent with oxidation of 30%–75% of Fe(II) to Fe(III),

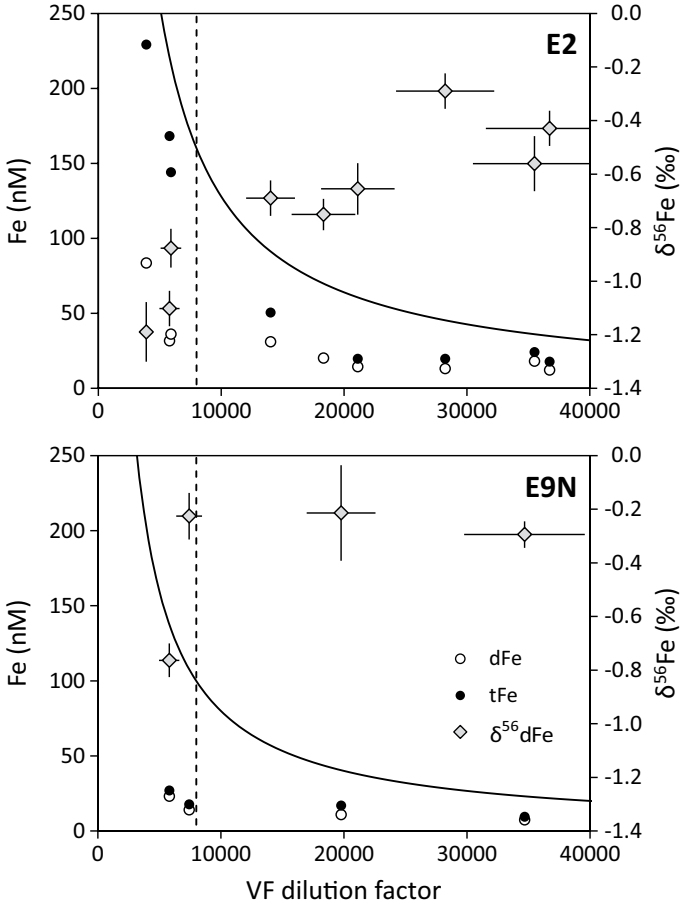

Figure 1. Evolution of dissolved Fe (dFe), total Fe (tFe = dFe + particulate Fe), calculated tFe (solid black line), and δ^{56}Fe of dFe during mixing (the calculation of the vent fluid, VF, dilution factor is described in the Data Repository [see footnote 1]). Vertical dashed line indicates the approximate boundary between the buoyant plume and the neutrally buoyant plume. Error bars on δ^{56}Fe indicate 2 standard deviations of 2 replicate analyses, or the external reproducibility, whichever is highest. Error bars on the dilution factor are ~14% (propagated error of the measured dMn concentrations in the plume and background seawater; see Table DR3 in the Data Repository).

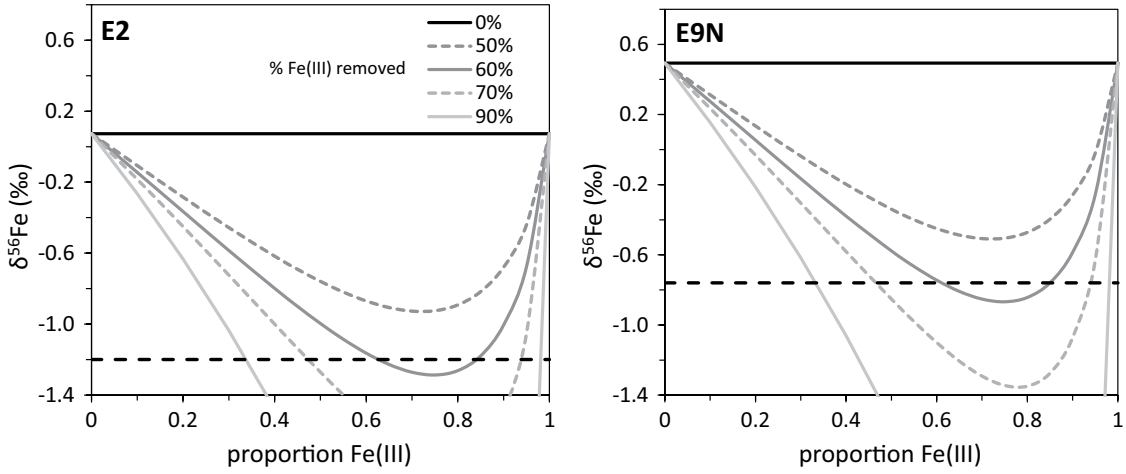

Figure 2. Evolution of δ^{56}Fe in the buoyant plume due to oxidation of Fe(II) to Fe(III) as a function of Fe(III) removal from the dissolved phase. Initial dFe(II) (d—dissolved) composition (after removal of Fe sulfides) is +0.07‰ at vent site E2, and +0.49‰ at vent site E9N in the East Scotia Sea. Dashed lines represent the measured isotopic composition of the least dilute sample collected from within the buoyant part of the hydrothermal plume.

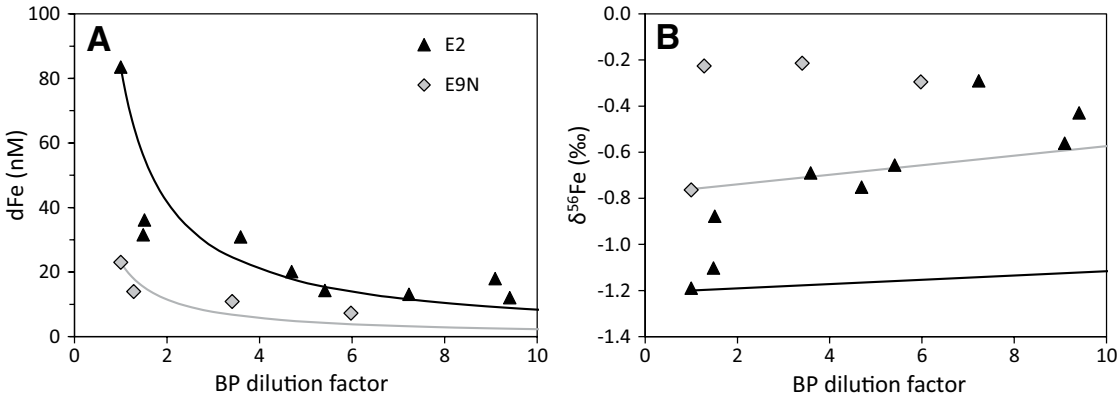

Figure 3. A: Evolution of dissolved Fe (dFe) concentrations in the buoyant plume (BP; the calculation of the BP dilution factor is described in the Data Repository; see footnote 1). B: Evolution of δ^{56}Fe. The evolution of dFe and δ^{56}Fe is modeled assuming conservative mixing between the least dilute BP sample (83 nM Fe, –1.2‰ for vent site E2 in the East Scotia Sea, and 23 nM Fe, –0.76‰ for vent site E9N, respectively) and background seawater (Weddell Sea Deep Water, 0.7 nM Fe, –0.1‰; Abadie et al., 2017).

with removal of >50% of the Fe(III) produced, at both E2 and E9N. The average proportion of tFe present as dFe in the buoyant plume (~50%; Fig. 1) is also consistent with the modeled amount of Fe(III) precipitation.

As the plume moves upward through the water column it continues to mix with seawater until the density within the plume equals that of surrounding seawater, at which point it spreads out to form the neutrally buoyant plume. During this process, dFe decreases and δ^{56}Fe increases. The most dilute part of the neutrally buoyant plume sampled at E2 has dFe ≈15 nM and δ^{56}Fe ≈ –0.5‰; at E9N dFe ≈7 nM and δ^{56}Fe ≈ –0.3‰. By contrast, background seawater (Weddell Sea Deep Water) has dFe ≈ 0.7 nM and δ^{56}Fe ≈ –0.1‰ (Abadie et al., 2017). However, although the decrease in dFe concentrations in the neutrally buoyant plume is broadly consistent with simple mixing between the buoyant plume and surrounding seawater, mixing cannot explain the evolution of δ^{56}Fe, because measured δ^{56}Fe values are higher than predicted (Fig. 3).

Relatively high δ^{56}Fe values cannot be attributed to limited fallout of Fe sulfide nanoparticles (Yücel et al., 2011), because these would have to have unrealistically low δ^{56}Fe (<–7.5‰) to reproduce the δ^{56}Fe values we measure for dFe in the neutrally buoyant plume. Our data therefore imply that a small proportion of hydrothermal Fe is stabilized within the <0.2 µm size fraction. This Fe could be in the form of colloidal Fe oxyhydroxides and/or Fe sulfide nanoparticles, or Fe complexed by ligands (FeL) (Yücel et al., 2011; Hawkes et al., 2013; Fitzsimmons et al., 2016). Studies of Fe speciation in the neutrally buoyant plumes from the East Scotia Ridge indicate that ~50% of dFe is in the colloidal fraction and ~30% of dFe is in the form of FeL (Hawkes et al., 2013). Relatively high δ^{56}Fe values in the neutrally buoyant plume may therefore reflect exchange between these dFe species, and labile Fe in the particulate fraction (e.g., neoformed FeOOH particles, adsorbed Fe; e.g., Ellwood et al., 2015).

IMPLICATIONS

Our data demonstrate that the δ^{56}Fe value of hydrothermal Fe stabilized in the dissolved fraction and delivered to the East Scotia Sea in the Southern Ocean is –0.5‰ (E2) and –0.3‰ (E9N), significantly higher than the value assigned (–1.35‰) in a recent study that aimed to quantify dissolved Fe sources to a North Atlantic transect (Conway and John, 2014). Our work shows that this value is critically dependent on the δ^{56}Fe value of the hydrothermal fluid, but also on the proportion of the Fe that precipitates as sulfides immediately on venting; the higher this is (e.g., E9N), the higher the δ^{56}Fe value of the stabilized dFe. Nevertheless, the δ^{56}Fe value of stabilized hydrothermal Fe from both vent sites in the East Scotia Sea is distinct from the background seawater (Weddell Sea Deep Water), as well as from other water masses surrounding mid-ocean ridges, and from other deep-ocean Fe sources (Fig. 4). There is, however, potential for overlap with the δ^{56}Fe signature of Fe derived from reducing sediments.

While our study confirms the importance of sulfide precipitation and Fe oxidation for setting the δ^{56}Fe value of hydrothermal iron delivered to the ocean interior, it also reveals the possibility for FeL complexation and continued exchange of Fe between dFe and particulate Fe. Understanding the physicochemical speciation of dFe remains essential for quantifying the longevity of hydrothermal iron and for modeling climate.

ACKNOWLEDGMENTS

This work was supported by UK Natural Environment Research Council (NERC) National Capability funds and the Graduate School of the National Oceanography Centre, Southampton. Research cruises JC042 and JC055 were funded by NERC consortium grant NE/D01249X/1. We thank the Captain and crew of RRS *James Cook* for support on both cruises. We also thank D. Green and B. Alker for shipboard and onshore laboratory assistance, K. Nakamura for the loan of his Eh sensor, and two anonymous reviewers for their considered and constructive reviews.

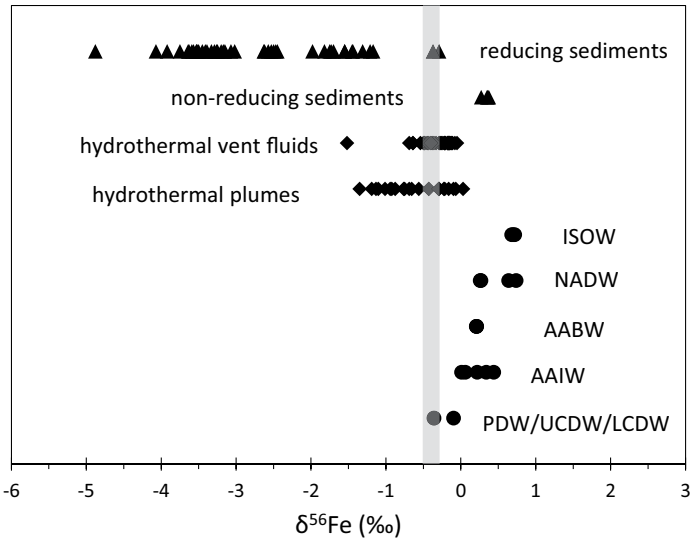

Figure 4. Range of δ^{56}Fe values of dissolved Fe (dFe) for deep-water sources, compared to δ^{56}Fe values for water masses bathing the world's mid-ocean ridges. ISOW—Iceland Scotland Overflow Water; NADW—North Atlantic Deep Water; AABW—Antarctic Bottom Water; AAIW—Antarctic Intermediate Water; PDW—Pacific Deep Water; UCDW—Upper Circumpolar Deep Water; LCDW—Lower Circumpolar Deep Water. Gray vertical band shows δ^{56}Fe of stabilized dFe supplied from hydrothermal plumes in the East Scotia Sea (–0.5‰ to –0.3‰). Data for reducing sediments are from John and Adkins (2012) and Severmann et al. (2011); core top and water column data from above nonreducing sediments are from Homoky et al. (2013), Labatut et al. (2014) and Radic et al. (2011); data for hydrothermal fluids are from Beard et al. (2003), Bennett et al. (2009), Rouxel et al. (2008) and Severmann et al. (2004); data for hydrothermal plumes are from Conway and John (2014) and this study; ISOW data are from Conway and John (2014); NADW data are from Conway and John (2014) and Conway et al. (2016); AABW data are from Lacan et al. (2008) and Conway et al. (2016); AAIW data are fom Labatut et al. (2014) and Radic et al. (2011); PDW, UCDW and LCDW data are from Conway and John (2015).

REFERENCES CITED

Abadie, C., Lacan, F., Radic, A., Pradoux, C., Poitrasson, F., 2017, Iron isotopes reveal distinct dissolved iron sources and pathways in the intermediate versus deep Southern Ocean: Proceedings of the National Academy of Sciences of the United States of America, doi:10.1073/pnas.1603107114 (in press).

Beard, B.L., Johnson, C.M., Von Damm, K.L., and Poulson, R.L., 2003, Iron isotope constraints on Fe cycling and mass balance in oxygenated Earth oceans: Geology, v. 31, p. 629–632, doi:10.1130/0091-7613(2003)031<0629:IICOFC>2.0.CO;2.

Bennett, S.A., Achterberg, E.P., Connelly, D.P., Statham, P.J., Fones, G.R., and German, C.R., 2008, The distribution and stabilisation of dissolved Fe in deep-sea hydrothermal plumes: Earth and Planetary Science Letters, v. 270, p. 157–167, doi:10.1016/j.epsl.2008.01.048.

Bennett, S.A., Rouxel, O., Schmidt, K., Garbe-Schönberg, D., Statham, P.J., and German, C.R., 2009, Iron isotope fractionation in a buoyant hydrothermal plume, 5°S Mid-Atlantic Ridge: Geochimica et Cosmochimica Acta, v. 73, p. 5619–5634, doi:10.1016/j.gca.2009.06.027.

Boyd, P.W., and Ellwood, M.J., 2010, The biogeochemical cycle of iron in the ocean: Nature Geoscience, v. 3, p. 675–682, doi:10.1038/ngeo964.

Conway, T.M., and John, S.G., 2014, Quantification of dissolved iron sources to the North Atlantic Ocean: Nature, v. 511, p. 212–215, doi:10.1038/nature13482.

Conway, T.M., and John, S.G., 2015, The cycling of iron, zinc and cadmium in the North East Pacific Ocean—Insights from stable isotopes: Geochimica et Cosmochimica Acta, v. 164, p. 262–283, doi:10.1016/j.gca.2015.05.023.

Conway, T.M., John, S.G., and Lacan, F., 2016, Intercomparison of dissolved iron isotope profiles from reoccupation of three GEOTRACES stations in the Atlantic Ocean: Marine Chemistry, v. 183, p. 50–61, doi:10.1016/j.marchem.2016.04.007 (erratum available at http://dx.doi.org/10.1016/j.marchem.2016.06.005).

Ellwood, M.J., Hutchins, D.A., Lohan, M.C., Milne, A., Nasemann, P., Nodder, S.D., Sander, S.G., Strzepek, R., Wilhelm, S.W., and Boyd, P.W., 2015, Iron stable isotopes track pelagic iron cycling during a subtropical phytoplankton bloom: National Academy of Sciences Proceedings, v. 112, p. E15–E20, doi:10.1073/pnas.1421576112.

Field, M.P., and Sherrell, R.M., 2000, Dissolved and particulate Fe in a hydrothermal plume at 9°45' N, East Pacific Rise: Slow Fe (II) oxidation kinetics in Pacific plumes: Geochimica et Cosmochimica Acta, v. 64, p. 619–628, doi:10.1016/S0016-7037(99)00333-6.

Fitzsimmons, J.N., Boyle, E.A., and Jenkins, W.J., 2014, Distal transport of dissolved hydrothermal iron in the deep South Pacific Ocean: National Academy of Sciences Proceedings, v. 111, p. 16654–16661, doi:10.1073/pnas.1418778111.

Fitzsimmons, J.N., Conway, T.M., Lee, J.M., Kayser, R., Thyng, K.M., John, S.G., and Boyle, E.A., 2016, Dissolved iron and iron isotopes in the southeastern Pacific Ocean: Global Biogeochemical Cycles, v. 30, p. 1372–1395, doi:10.1002/2015GB005357.

Hawkes, J.A., Connelly, D.P., Gledhill, M., and Achterberg, E.P., 2013, The stabilisation and transportation of dissolved iron from high temperature hydrothermal vent systems: Earth and Planetary Science Letters, v. 375, p. 280–290, doi:10.1016/j.epsl.2013.05.047.

Hawkes, J.A., Connelly, D.P., Rijkenberg, M.J.A., and Achterberg, E.P., 2014, The importance of shallow hydrothermal island arc systems in ocean biogeochemistry: Geophysical Research Letters, v. 41, p. 942–947, doi:10.1002/2013GL058817.

Homoky, W.B., John, S.G., Conway, T.M., and Mills, R.A., 2013, Distinct iron isotopic signatures and supply from marine sediment dissolution: Nature Communications, v. 4, 2143, doi:10.1038/ncomms3143.

James, R.H., Green, D.R.H., Stock, M.J., Alker, B.J., Banerjee, N.R., Cole, C., German, C.R., Huvenne, V.A.I., Powell, A.M., and Connelly, D.P., 2014, Composition of hydrothermal fluids and mineralogy of associated chimney material on the East Scotia Ridge back-arc spreading centre: Geochimica et Cosmochimica Acta, v. 139, p. 47–71, doi:10.1016/j.gca.2014.04.024.

John, S.G., and Adkins, J., 2012, The vertical distribution of iron stable isotopes in the North Atlantic near Bermuda: Global Biogeochemical Cycles, v. 26, GB2034, doi:10.1029/2011GB004043.

Kleint, C., Hawkes, J.A., Sander, S.G., and Koschinsky, A., 2016, Voltammetric investigation of hydrothermal iron speciation: Frontiers in Marine Science, v. 3, p. 75, doi:10.3389/fmars.2016.00075.

Labatut, M., Lacan, F., Pradoux, C., Chmeleff, J., Radic, A., Murray, J.W., Poitrasson, F., Johansen, A.M., and Thil, F., 2014, Iron sources and dissolved-particulate interactions in the seawater of the Western Equatorial Pacific, iron isotope perspectives: Global Biogeochemical Cycles, v. 28, p. 1044–1065, doi:10.1002/2014GB004928.

Lacan, F., Radic, A., Jeandel, C., Poitrasson, F., Sarthou, G., Pradoux, C., and Freydier, R., 2008, Measurement of the isotopic composition of dissolved iron in the open ocean: Geophysical Research Letters, v. 35, L24610, doi:10.1029/2008GL035841.

Martin, J.H., Fitzwater, S.E., and Gordon, R.M., 1990, Iron deficiency limits phytoplankton growth in Antarctic waters: Global Biogeochemical Cycles, v. 4, p. 5–12, doi:10.1029/GB004i001p00005.

Pollard, R.T., et al., 2009, Southern Ocean deep-water carbon export enhanced by natural iron fertilization: Nature, v. 457, p. 577–580, doi:10.1038/nature07716.

Radic, A., Lacan, F., and Murray, J.W., 2011, Iron isotopes in the seawater of the equatorial Pacific Ocean: New constraints for the oceanic iron cycle: Earth and Planetary Science Letters, v. 306, p. 1–10, doi:10.1016/j.epsl.2011.03.015.

Resing, J.A., Sedwick, P.N., German, C.R., Jenkins, W.J., Moffett, J.W., Sohst, B.M., and Tagliabue, A., 2015, Basin-scale transport of hydrothermal dissolved metals across the South Pacific Ocean: Nature, v. 523, p. 200–203, doi:10.1038/nature14577.

Rouxel, O., Shanks, W.C., Bach, W., and Edwards, K.J., 2008, Integrated Fe- and S-isotope study of seafloor hydrothermal vents at East Pacific rise 9–10°N: Chemical Geology, v. 252, p. 214–227, doi:10.1016/j.chemgeo.2008.03.009.

Rouxel, O., Toner, B.M., Manganini, S.J., and German, C.R., 2016, Geochemistry and iron isotope systematics of hydrothermal plume fall-out at East Pacific Rise 9°50′N: Chemical Geology, v. 441, p. 212–234, doi:10.1016/j.chemgeo.2016.08.027.

Roy, M., Rouxel, O., Martin, J.B., and Cable, J.E., 2012, Iron isotope fractionation in a sulfide-bearing subterranean estuary and its potential influence on oceanic Fe isotope flux: Chemical Geology, v. 300–301, p. 133–142, doi:10.1016/j.chemgeo.2012.01.022.

Rudnicki, M.D., and Elderfield, H., 1993, A chemical model of the buoyant and neutrally buoyant plume above the TAG vent field, 26°N, Mid-Atlantic Ridge: Geochimica et Cosmochimica Acta, v. 57, p. 2939–2957, doi:10.1016/0016-7037(93)90285-5.

Saito, M.A., Noble, A.E., Tagliabue, A., Goepfert, T.J., Lamborg, C.H., and Jenkins, W.J., 2013, Slow-spreading submarine ridges in the South Atlantic as a significant oceanic iron source: Nature Geoscience, v. 6, p. 775–779, doi:10.1038/ngeo1893.

Severmann, S., Johnson, C.M., Beard, B.L., German, C.R., Edmonds, H.N., Chiba, H., and Green, D.R.H., 2004, The effect of plume processes on the Fe isotope composition of hydrothermally derived Fe in the deep ocean as inferred from the Rainbow vent site, Mid-Atlantic Ridge, 36°14′N: Earth and Planetary Science Letters, v. 225, p. 63–76, doi:10.1016/j.epsl.2004.06.001.

Severmann, S., McManus, J., Berelson, W.M., and Hammond, D.E., 2010, The continental shelf benthic iron flux and its isotope composition: Geochimica et Cosmochimica Acta, v. 74, p. 3984–4004, doi:10.1016/j.gca.2010.04.022.

Statham, P.J., German, C.R., and Connelly, D.P., 2005, Iron(II) distribution and oxidation kinetics in hydrothermal plumes at the Kairei and Edmond vent sites, Indian Ocean: Earth and Planetary Science Letters, v. 236, p. 588–596, doi:10.1016/j.epsl.2005.03.008.

Tagliabue, A., Aumont, O., and Bopp, L., 2014, The impact of different external sources of iron on the global carbon cycle: Geophysical Research Letters, v. 41, p. 920–926, doi:10.1002/2013GL059059.

Tagliabue, A., et al., 2010, Hydrothermal contribution to the oceanic dissolved iron inventory: Nature Geoscience, v. 3, p. 252–256, doi:10.1038/ngeo818.

Watson, A.J., Bakker, D.C.E., Ridgwell, A.J., Boyd, P.W., and Law, C.S., 2000, Effect of iron supply on Southern Ocean CO_2 uptake and implications for glacial atmospheric CO_2: Nature, v. 407, p. 730–733, doi:10.1038/35037561.

Welch, S.A., Beard, B.L., Johnson, C.M., and Braterman, P.S., 2003, Kinetic and equilibrium Fe isotope fractionation between aqueous Fe(II) and Fe(III): Geochimica et Cosmochimica Acta, v. 67, p. 4231–4250, doi:10.1016/S0016-7037(03)00266-7.

Yücel, M., Gartman, A., Chan, C.S., and Luther, G., 2011, Hydrothermal vents as a kinetically stable source of iron-sulphide-bearing nanoparticles to the ocean: Nature Geoscience, v. 4, p. 367–371, doi:10.1038/ngeo1148.

Manuscript received 1 August 2016
Revised manuscript received 11 December 2016
Manuscript accepted 13 December 2016

Printed in USA